



Zr³⁺ ion as a prospective terahertz atomic clockJyoti ¹, A. Chakraborty,^{2,3} Yan-mei Yu,^{4,5} Jingbiao Chen,⁶ Bindiya Arora ^{1,7,*} and B. K. Sahoo^{2,†}¹*Department of Physics, Guru Nanak Dev University, Amritsar, Punjab 143005, India*²*Atomic, Molecular and Optical Physics Division, Physical Research Laboratory, Navrangpura, Ahmedabad 380009, India*³*Indian Institute of Technology Gandhinagar, Palaj, Gandhinagar 382355, India*⁴*Beijing National Laboratory for Condensed Matter Physics, Institute of Physics, Chinese Academy of Sciences, Beijing 100190, China*⁵*University of Chinese Academy of Sciences, Beijing 100049, China*⁶*Institute of Quantum Electronics, School of Electronics, Peking University, Beijing 100871, China*⁷*Perimeter Institute for Theoretical Physics, Waterloo, Ontario, Canada N2L 2Y5*

(Received 25 May 2023; accepted 25 July 2023; published 10 August 2023)

We demonstrate that the transition between the fine-structure splitting of the ground state of triply ionized zirconium (Zr IV) is suitable for a terahertz (THz) atomic clock. Its transition frequency is about 37.52 THz and is mainly guided by the magnetic dipole (M1) transition, and it is accessible by a readily available laser. We suggest considering stable even isotopes of Zr and $M_J = \pm 1/2$ sublevels (i.e., $|4D_{3/2}, M_J = \pm 1/2\rangle \rightarrow |4D_{5/2}, M_J = \pm 1/2\rangle$ clock transition) for experimental advantage. By performing necessary calculations, we estimate possible systematics due to blackbody radiation and ac Stark, electric quadrupole, and second-order Zeeman shifts along with shifts due to the second-order Doppler effects. The proposed THz atomic clock could be very useful in quantum thermometry and frequency metrology.

DOI: [10.1103/PhysRevA.108.023115](https://doi.org/10.1103/PhysRevA.108.023115)**I. INTRODUCTION**

Atomic clocks are used to define the unit of time with such high precision that they can lose only 1 s over several billion years. They also serve as important tools to probe much fundamental physics, with applications ranging from probing the variation of fundamental physical constants [1] to relativistic geodesy [2,3], gravitational-wave detection [4–6], and the search for dark matter [7], and even go beyond the standard-model particle physics [8]. Most existing atomic clocks are based on either neutral atoms or singly charged ions and operate in both microwave and optical domains. Singly charged ions are suitable for carrying out many precise experiments with the advent of many cooling and trapping techniques. In fact, single trapped ¹⁷¹Yb⁺ [9] and Al⁺ [10] ions now provide clock frequencies with fractional uncertainties below 10⁻¹⁹. Ions are relatively easier to control using electromagnetic radiation to perform high-precision measurements. Atomic clocks operating at microwave and optical frequencies have advantages in their own right. The frequencies of these clocks differ by several orders of magnitude; thus, they can be applied in a diverse range of fields. From this point of view, it is desirable to attain atomic clocks operating between microwave and optical clock frequencies such as terahertz (THz) frequencies. Recent advancements in science and technology have demonstrated applications of various ingenious modes of THz electromagnetic radiation in sensing, spectroscopy, and communication [11] and for the analysis of interstellar

matter [12]. THz spectra have long been studied in the fields of astronomy and analytical science [11]. The implementation of absolute frequency standards in the THz domain considering fine-structure transition lines of Mg and Ca metastable triplet states was first proposed by Strumia in 1972 [13].

The salient feature of THz-range clock transition is that it is highly sensitive to blackbody radiations (BBR) and hence can be used in quantum thermometers, especially in remote-sensing satellites [14]. Major applications of the THz-frequency standard lie in new generations of navigation, sensing, and communication systems, especially when the GPS timing service becomes inadequate [15]. In addition, THz clocks are also crucial in the frequency calibration of various commercial THz instruments such as detectors, sources, and high-resolution THz spectrometers [16]. Making the switch from the optical frequency framework to THz technology to study astronomical phenomena has also become obvious because 98% of the photons emitted since the big bang and one half of the total luminosity of our galaxy comprise THz radiations [17,18]. Moreover, the implementation of THz clocks could play a vital role in the investigation of the unexplored universe as well as the instrumentation of astronomical objects, especially astronomical interferometers and next-generation space telescopes. Even though the precision of optical clocks is far better than THz-frequency metrology, clear insights into star formation and decay and thermal fluctuations in the environment due to the immense release of greenhouse gases [17] also require the realization of THz-frequency standards.

Recently, several transitions lying in the THz domain have drawn attention for consideration for atomic clocks. The generation of a tunable THz optical clock was demonstrated by

*bindiya.phy@gndu.ac.in

†bijaya@prl.res.in

Yamamoto *et al.* [19]. Further, magic wavelengths of THz clock transitions in alkaline-earth atoms, including Sr, Ca, and Mg, were identified between metastable triplet states by Zhou *et al.* [20]. The ac Stark shifts and magic wavelengths of THz clock transitions in barium were calculated by Yu *et al.* [21]. Two different molecular clocks probing carbonyl sulfide based on the sub-THz-frequency standard were realized by Wang *et al.* [22]. In 2019, Kim *et al.* analyzed a miniature timekeeping device with high affordability in a chip-scale terahertz carbonyl sulfide (OCS) clock [15], whereas THz-rate Kerr microresonator optical clockwork based on silicon nitride was performed by Drake *et al.* [23]. Wang *et al.* proposed chip-scale molecular clocks based on a complementary metal-oxide-semiconductor technique with selected OCS transitions [24] in 2020. Recently, Leung *et al.* [25] constructed a molecular clock using the vibrational levels of Sr₂ and achieved systematic uncertainty at the level of 10⁻¹⁴. In view of this, here, we propose a THz clock based on the M1 transition occurring between the 4D_{3/2} and 4D_{5/2} states of a Zr³⁺ ion. To support it, we estimate major systematic shifts in the proposed clock transition.

The outline of this paper is as follows: Sec. II presents the detailed proposal for our THz ion clock. Section III demonstrates the method used to evaluate atomic wave functions and matrix elements. Section IV presents the electric dipole (E1) and magnetic dipole (M1) polarizabilities used for estimating systematic effects. Section V discusses the dominant systematic shifts. Section VI compares the frequency standard using Zr³⁺ with existing THz clock proposals, and the conclusion of the study is given in Sec. VII. Unless we have stated explicitly otherwise, physical quantities are given in atomic units.

II. SCHEMATIC OF THE THz ⁹⁰Zr³⁺ CLOCK

Using various spectroscopic properties reported in our previous work [26], we find that the wavelength of the 4D_{3/2}–4D_{5/2} transition of Zr³⁺ is about λ₀ = 7.9955 μm, corresponding to a transition frequency of 37.52 THz. Also, the lifetime of the 4D_{5/2} state is reported to be ~47.38 s [27]. These two conditions are sufficient enough to consider the 4D_{3/2}–4D_{5/2} transition in Zr³⁺ as a possible clock transition. Among several isotopes of Zr, we find that ⁹⁰Zr₄₀ would be the most appropriate for consideration in the experiment. The reason is that this isotope has more than 51% natural abundance [28] and zero nuclear spin *I* and hence cannot introduce additional systematic effects when ⁹⁰Zr³⁺ interacts with the external magnetic field. Moreover, it can be trapped using electron-beam ion traps [29,30] and electron-cyclotron resonance accelerators [31] in the laboratory.

There are at least two ways one can measure the transition frequency of the 4D_{3/2}–4D_{5/2} transition in ⁹⁰Zr³⁺. One can follow the quantum logic principle by trapping this ion simultaneously with another ion like Mg⁺ or Ca⁺ along lines similar to the ²⁷Al⁺ ion clock to carry out the clock frequency measurement because they have similar charge-to-mass ratios [10,32]. A schematic diagram of the other possible setup is illustrated in Fig. 1. As can be seen in Fig. 1, the 4D_{5/2} state has a longer lifetime, so the desirable accumulation of the atomic

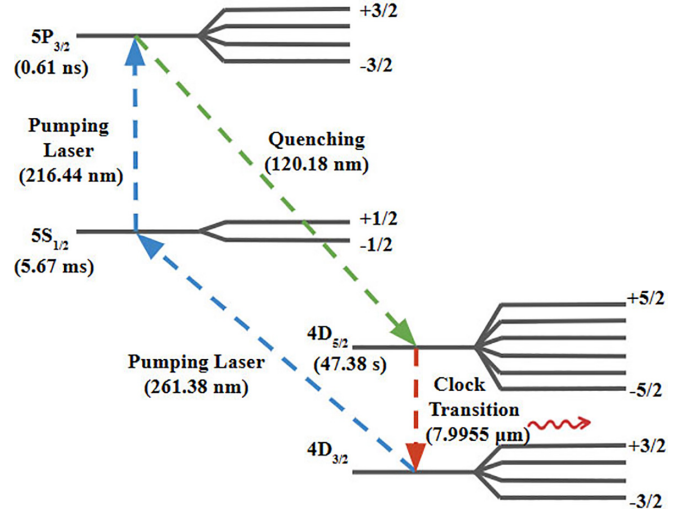


FIG. 1. Schematic of the clock frequency measurement setup using the Zr³⁺ ion. As shown, the 4D_{3/2}–4D_{5/2} transition is used for THz clock frequency measurement and 4D_{3/2} → 5S → 5P_{3/2} transitions are used for pumping the electrons to the excitation levels. The 5P_{3/2} → 4D_{5/2} decay channel is used to populate the upper level of the clock transition.

population can be achieved in this state. This can lead to a favorable population inversion condition between the 4D_{5/2} and 4D_{3/2} states. In this case, electrons can be pumped first from the ground state to the excited 5S_{1/2} state using a laser of 261.38 nm, which is far detuned from the clock transition at 7.9955 μm. To acquire population inversion at the 4D_{5/2} metastable state via spontaneous electric dipole emission, we aspire to again pump electrons from the 5S_{1/2} state to the 5P_{3/2} state using a second-stage laser of 216.44 nm. It should be noted that it would be desirable to pump electrons directly from the ground to the 5P_{3/2} state, but it is difficult to find a suitable laser to carry out this process. Our estimations suggest that the lifetime of the 5P_{3/2} state is about 0.61 ns with a 64% decay rate to the 4D_{5/2} state, which would be enough to carry out the measurement of the clock frequency for an atomic-clock experiment. A small population (~28%) of the 5S_{1/2} state due to the decay of electrons from the 5P_{3/2} state can be managed with the help of an applied pump laser of 216.44 nm. Nonetheless, decay from the 5S_{1/2} state to the 4D_{5/2} state is highly forbidden, so it will not have much impact on the clock frequency measurement. Thus, it is feasible to acquire population inversion between the 4D_{3/2} and 4D_{5/2} states via the M1 decay channel to observe a clock frequency of 37.52 THz. To achieve high stability and accuracy in this proposed THz clock scheme, usage of a feedback loop to control the energy difference between the 4D_{3/2} and 4D_{5/2} states is recommended. This feedback loop would adjust the static magnetic field applied to the ion trap to maintain a stable clock frequency over time [33].

III. METHOD OF EVALUATION

Accurate evaluation of the wave functions of the states involved in the clock transition is a prerequisite for the

determination of the systematic shifts to which the clock transition is sensitive. Therefore, we implement relativistic-coupled-cluster (RCC) theory for the precise computation of wave functions and thus the matrix elements. We incorporate higher-order correlations due to various physical effects such as the core-polarization and pair-correlation effects. The general formulation and potential applications of RCC theory can be found in many previous studies, including Refs. [34–38]. We give a brief outline of our employed RCC method below.

We consider the Dirac-Coulomb (DC) Hamiltonian in our RCC method, which, in atomic units, is given by

$$H_{\text{DC}} = \sum_{i=1}^{N_e} [c\vec{\alpha}_D \cdot \vec{p}_i + (\beta - 1)c^2 + V_n(r_i)] + \sum_{i>j} \frac{1}{r_{ij}}, \quad (1)$$

where N_e is the number of electrons in the atom, c is the speed of light, $\vec{\alpha}_D$ and β are the Dirac matrices, $V_n(r)$ is the nuclear potential, and r_{ij} is the interelectronic distances between electrons located at r_i and r_j .

In the (R)CC theory ansatz, the wave function of a many-electron system can be expressed in terms of the mean-field wave function $|\Phi_0\rangle$ of an atomic state and cluster operator T as [39]

$$|\Psi_0\rangle = e^T |\Phi_0\rangle. \quad (2)$$

In the above equation, the mean-field wave function can be computed using the Dirac-Fock (DF) method. Following V^{N-1} potential formalism, we first solve the DF equation for closed-shell configurations ($[4p^6]$) to get $|\Phi_0\rangle$, and then a valence orbital v is added to obtain the DF wave function of $[4p^6]v$ by defining [40]

$$|\Phi_v\rangle = a_v^\dagger |\Phi_0\rangle, \quad (3)$$

where a_v^\dagger is the creation operator for the valence electron. Now, the wave function of an atomic state with a closed-shell electronic configuration and a valence orbital can be expressed as [41]

$$|\Psi_v\rangle = e^T \{1 + S_v\} |\Phi_v\rangle, \quad (4)$$

where T is the RCC operator that accounts for the excitations of core electrons to virtual orbitals and S_v is the RCC operator that excites the valence orbital to a virtual orbital. Amplitudes of the T and S_v operators are obtained by solving the standard RCC equations. In our work, we consider only the singly and doubly excited-state configurations in our RCC theory (the RCCSD method) by expressing [41]

$$T = T_1 + T_2, \quad S_v = S_{1v} + S_{2v}. \quad (5)$$

Here, the excitation operators take into account excitations from both core and valence orbitals of the DF wave functions of the Zr³⁺ ion, and they are defined using the second quantized operators as [42]

$$\begin{aligned} T_1 &= \sum_{p,a} \rho_{pa} a_p^\dagger a_a, & T_2 &= \frac{1}{4} \sum_{pq,ab} \rho_{pqab} a_p^\dagger a_q^\dagger a_b a_a, \\ S_{1v} &= \sum_{m \neq a} \rho_{pa} a_p^\dagger a_v, & S_{2v} &= \frac{1}{2} \sum_{pq,a} \rho_{pqva} a_p^\dagger a_q^\dagger a_a a_v, \end{aligned} \quad (6)$$

where the indices p and q range over all possible virtual orbitals and the indices a and b range over all occupied core orbitals. The quantities ρ depict excitation coefficients.

Consequently, the matrix elements for the operator \hat{O} between states k and v with corresponding wave functions $|\Psi_v\rangle$ and $|\Psi_k\rangle$ can be evaluated by [43]

$$\begin{aligned} O_{vk} &= \frac{\langle \Psi_v | \hat{O} | \Psi_k \rangle}{\sqrt{\langle \Psi_v | \Psi_v \rangle \langle \Psi_k | \Psi_k \rangle}} \\ &= \frac{\langle \Phi_v | \{S_v^\dagger + 1\} \bar{O} \{1 + S_k\} | \Phi_k \rangle}{\langle \Phi_v | \{S_v^\dagger + 1\} \bar{N} \{1 + S_k\} | \Phi_k \rangle}, \end{aligned} \quad (7)$$

where $\bar{O} = e^{T^\dagger} \hat{O} e^T$ and $\bar{N} = e^{T^\dagger} e^T$. Both \bar{O} and \bar{N} are nonterminating series. In the above expression, the operator \hat{O} can be replaced by electric dipole (E1), magnetic dipole (M1), and electric quadrupole (E2) operators depending upon the matrix elements that need to be evaluated.

IV. DIPOLE POLARIZABILITIES

Interactions between the electromagnetic fields and an atomic system cause shifts in the energy levels of the atomic system. The first-order effect due to the electric field vanishes, and the next dominant second-order shift can be described with knowledge of the E1 polarizabilities. In fact, the BBR shift of an atomic energy level can be estimated using its static E1 polarizability. Since the first-order magnetic-field effects on the atomic energy levels in a clock experiment are canceled out by carrying out measurement suitably, the second-order effects can be estimated with knowledge of the M1 polarizabilities. Thus, it is evident that accurate calculations of E1 and M1 polarizabilities are essential in order to estimate the possible systematics in the clock states of the considered atomic system. Here, we use the dominant E1 and M1 matrix elements from the RCC method, and excitation energies are taken from the NIST database [44] to determine these quantities. The details of these calculations and the obtained results are discussed below.

A. E1 polarizabilities

The total dynamic dipole polarizability of an atomic state $|J_v, M_J\rangle$ in the presence of a linearly polarized laser can be expressed as [45]

$$\alpha_v^{\text{E1}}(\omega) = \alpha_{v0}^{\text{E1}}(\omega) + \frac{3M_J^2 - J_v(J_v + 1)}{J_v(2J_v - 1)} \alpha_{v2}^{\text{E1}}(\omega). \quad (8)$$

Here, $\alpha_{v0}^{\text{E1}}(\omega)$ and $\alpha_{v2}^{\text{E1}}(\omega)$ represent the scalar and tensor parts of the total dipole polarizability of state v with angular momentum J_v and its corresponding magnetic projection M_J . $\alpha_{v0}^{\text{E1}}(\omega)$ and $\alpha_{v2}^{\text{E1}}(\omega)$ do not depend on M_J and can easily be calculated by using [45]

$$\begin{aligned} \alpha_{v0}^{\text{E1}}(\omega) &= -\frac{1}{3(2J_v + 1)} \sum_k | \langle J_v || \hat{O}^{\text{E1}} || J_k \rangle |^2 \\ &\quad \times \left[\frac{1}{\delta E_{vk} + \omega} + \frac{1}{\delta E_{vk} - \omega} \right] \end{aligned} \quad (9)$$

TABLE I. Contributions of different E1 matrix elements d to the static dipole polarizabilities (in a.u.) of the $4D_{3/2}$ and $4D_{5/2}$ states of Zr^{3+} . Percentage deviations in the results $\delta(\%)$ are given with respect to the values obtained using the RMBPT3 method.

| $4D_{3/2}$ | | | | $4D_{5/2}$ | | | |
|-------------------------------------|--------|---------------|---------------|-------------------------------------|--------|---------------|---------------|
| Transition | d | α_{w0} | α_{w2} | Transition | d | α_{v0} | α_{v2} |
| $4D_{3/2} \rightarrow 5P_{1/2}$ | 1.465 | 0.9577 | -0.9577 | $4D_{5/2} \rightarrow 5P_{3/2}$ | -1.955 | 1.1201 | -1.1201 |
| $4D_{3/2} \rightarrow 6P_{1/2}$ | -0.257 | 0.0142 | -0.0142 | $4D_{5/2} \rightarrow 6P_{3/2}$ | -0.362 | 0.0188 | -0.0188 |
| $4D_{3/2} \rightarrow 7P_{1/2}$ | -0.121 | 0.0026 | -0.0026 | $4D_{5/2} \rightarrow 7P_{3/2}$ | -0.175 | 0.0036 | -0.0036 |
| $4D_{3/2} \rightarrow 8P_{1/2}$ | -0.073 | 0.0009 | -0.0009 | $4D_{5/2} \rightarrow 8P_{3/2}$ | 0.108 | 0.0013 | -0.0013 |
| $4D_{3/2} \rightarrow 9P_{1/2}$ | -0.050 | 0.0004 | -0.0004 | $4D_{5/2} \rightarrow 9P_{3/2}$ | 0.074 | 0.0006 | -0.0006 |
| $4D_{3/2} \rightarrow 10P_{1/2}$ | 0.038 | 0.0002 | -0.0002 | $4D_{5/2} \rightarrow 10P_{3/2}$ | -0.051 | 0.0003 | -0.0003 |
| $4D_{3/2} \rightarrow 5P_{3/2}$ | -0.642 | 0.1788 | 0.1430 | $4D_{5/2} \rightarrow 4F_{5/2}$ | 0.549 | 0.0466 | 0.0534 |
| $4D_{3/2} \rightarrow 6P_{3/2}$ | -0.120 | 0.0030 | 0.0024 | $4D_{5/2} \rightarrow 5F_{5/2}$ | -0.209 | 0.0053 | 0.0061 |
| $4D_{3/2} \rightarrow 7P_{3/2}$ | -0.058 | 0.0006 | 0.0005 | $4D_{5/2} \rightarrow 6F_{5/2}$ | 0.092 | 0.0009 | 0.0011 |
| $4D_{3/2} \rightarrow 8P_{3/2}$ | 0.036 | 0.0002 | 0.0002 | $4D_{5/2} \rightarrow 4F_{7/2}$ | -2.461 | 0.9357 | -0.3340 |
| $4D_{3/2} \rightarrow 9P_{3/2}$ | 0.025 | 0.0001 | 0.0001 | $4D_{5/2} \rightarrow 5F_{7/2}$ | -0.960 | 0.1123 | -0.0401 |
| $4D_{3/2} \rightarrow 10P_{3/2}$ | -0.022 | 0.0001 | 0.0001 | $4D_{5/2} \rightarrow 6F_{7/2}$ | -0.466 | 0.0237 | -0.0085 |
| $4D_{3/2} \rightarrow 4F_{5/2}$ | -2.027 | 0.9450 | -0.1900 | | | | |
| $4D_{3/2} \rightarrow 5F_{5/2}$ | 0.779 | 0.1105 | -0.0221 | | | | |
| $4D_{3/2} \rightarrow 6F_{5/2}$ | -0.359 | 0.0210 | -0.0042 | | | | |
| $4D_{3/2} \rightarrow 7F_{5/2}$ | -0.170 | 0.0049 | -0.0010 | | | | |
| $4D_{3/2} \rightarrow 8F_{5/2}$ | 0.022 | 0.0001 | 0.0000 | | | | |
| $\alpha_{\text{Main}}^{\text{val}}$ | | 2.2403 | -1.0848 | $\alpha_{\text{Main}}^{\text{val}}$ | | 2.2692 | -1.5492 |
| $\alpha_{\text{Tail}}^{\text{val}}$ | | 0.1752 | -0.0409 | $\alpha_{\text{Tail}}^{\text{val}}$ | | 0.2442 | -0.0787 |
| α^c | | 2.9771 | | α^c | | 2.9771 | |
| α^{vc} | | -0.2431 | 0.1629 | α^{vc} | | -0.2649 | 0.2649 |
| Total | | 5.1495 | -0.9628 | Total | | 5.2256 | -1.3630 |
| $\delta(\%)$ | | 1.91 | 5.89 | $\delta(\%)$ | | 1.75 | 12.03 |

and

$$\begin{aligned}
\alpha_{v2}^{\text{E1}}(\omega) &= 2\sqrt{\frac{5J_v(2J_v-1)}{6(J_v+1)(2J_v+3)(2J_v+1)}} \\
&\times \sum_k (-1)^{J_k+J_v+1} \begin{Bmatrix} J_v & 2 & J_v \\ 1 & J_k & 1 \end{Bmatrix} |\langle J_v || \hat{O}^{\text{E1}} || J_k \rangle|^2 \\
&\times \left[\frac{1}{\delta E_{vk} + \omega} + \frac{1}{\delta E_{vk} - \omega} \right]. \quad (10)
\end{aligned}$$

Here, $|\langle J_v || \hat{O}^{\text{E1}} || J_k \rangle|$ are reduced electric dipole matrix elements, with J_k being the angular momentum of intermediate state k . The term in curly brackets refers to 6- j symbols.

Moreover, the dipole polarizability of any atom with a closed core and one electron in the outermost shell can also be estimated by evaluating the core, core-valence, and valence correlation contributions [46], i.e.,

$$\alpha_v^{\text{E1}}(\omega) = \alpha^c(\omega) + \alpha^{\text{vc}}(\omega) + \alpha^{\text{val}}(\omega), \quad (11)$$

where $\alpha^c(\omega)$, $\alpha^{\text{vc}}(\omega)$, and $\alpha^{\text{val}}(\omega)$ are the core, core-valence, and valence correlation contributions, respectively. Here, the tensor component of the core and valence-core contributions is zero. Further, our valence contribution [$\alpha^{\text{val}}(\omega)$] to the polarizability is divided into two parts, the main part ($\alpha_{\text{Main}}^{\text{val}}$) and the tail part ($\alpha_{\text{Tail}}^{\text{val}}$), in which the first few dominant and the other less dominant transitions of Eqs. (9) and (10) are included, respectively.

The results for the static dipole polarizabilities ($\omega = 0$) of the considered $4D_{3/2}$ and $4D_{5/2}$ states are listed in

Table I, and the dynamic dipole polarizabilities of the two states in the presence of a 216.44-nm pumping laser are tabulated in Table II. These results are estimated by using the matrix elements from the RCCSD method. In order to cross-check the results, we also estimate matrix elements using the random-phase approximation that accounts for core-polarization effects to all orders and separately adding other correlation effects through the Brückner orbitals, structural radiation, and normalizations of wave functions in the third-order relativistic many-body perturbation theory (denoted as the RMBPT3 method). Percentage deviations $\delta(\%)$ in the E1 polarizability results are also given in Tables I and II. It can be seen from Table I that the $4D_{3/2} \rightarrow 5P_{1/2,3/2}$ and $4D_{3/2} \rightarrow (4, 5)F_{5/2}$ transitions contribute mainly to the valence part of the static polarizability of the $4D_{3/2}$ state. Similarly, the $4D_{5/2} \rightarrow 5P_{3/2}$ and $4D_{5/2} \rightarrow (4, 5)F_{7/2}$ transitions seem to be dominant in the main part of the valence contribution of the static dipole polarizability of the $4D_{5/2}$ state. The total static scalar dipole polarizabilities of the $4D_{3/2}$ and $4D_{5/2}$ states of the Zr^{3+} ion are found to be 5.1495 and 5.2256 a.u., respectively. Table I also depicts that a maximum of 12% deviation is obtained in the tensor part of the polarizability because the RCCSD method includes higher-order correlations compared to the RMBPT3 method.

In a similar manner, we tabulate our dynamic dipole polarizability results for the linearly polarized pumping laser with a wavelength of 216.44 nm in Table II. On the basis of Eq. (8), we determine the total dipole polarizabilities of the ground $|4D_{3/2}, M_J = \pm 1/2\rangle$ and excited $|4D_{5/2}, M_J = \pm 1/2\rangle$ states of the Zr^{3+} ion for the 216.44-nm pumping

TABLE II. Contributions of different E1 matrix elements d to the dynamic dipole polarizabilities (in a.u.) of the $4D_{3/2}$ and $4D_{5/2}$ states of Zr³⁺ for a pumping laser with a wavelength of 216.44 nm. Percentage deviations in the results $\delta(\%)$ are given with respect to the RMBPT3 results.

| $4D_{3/2}$ | | | | $4D_{5/2}$ | | | |
|-------------------------------------|--------|-----------------------|-----------------------|-------------------------------------|--------|-----------------------|-----------------------|
| Transition | d | $\alpha_{w0}(\omega)$ | $\alpha_{w2}(\omega)$ | Transition | d | $\alpha_{v0}(\omega)$ | $\alpha_{v2}(\omega)$ |
| $4D_{3/2} \rightarrow 5P_{1/2}$ | -1.465 | 1.4035 | -1.4035 | $4D_{5/2} \rightarrow 5P_{3/2}$ | -1.955 | 1.6193 | -1.6193 |
| $4D_{3/2} \rightarrow 6P_{1/2}$ | -0.257 | 0.0154 | -0.0154 | $4D_{5/2} \rightarrow 6P_{3/2}$ | -0.362 | 0.0203 | -0.0203 |
| $4D_{3/2} \rightarrow 7P_{1/2}$ | -0.121 | 0.0027 | -0.0027 | $4D_{5/2} \rightarrow 7P_{3/2}$ | -0.175 | 0.0038 | -0.0038 |
| $4D_{3/2} \rightarrow 8P_{1/2}$ | -0.073 | 0.0009 | -0.0009 | $4D_{5/2} \rightarrow 8P_{3/2}$ | 0.108 | 0.0014 | -0.0014 |
| $4D_{3/2} \rightarrow 9P_{1/2}$ | -0.050 | 0.0004 | -0.0004 | $4D_{5/2} \rightarrow 9P_{3/2}$ | 0.074 | 0.0006 | -0.0006 |
| $4D_{3/2} \rightarrow 10P_{1/2}$ | 0.038 | 0.0002 | -0.0002 | $4D_{5/2} \rightarrow 10P_{3/2}$ | -0.051 | 0.0003 | -0.0003 |
| $4D_{3/2} \rightarrow 5P_{3/2}$ | -0.642 | 0.2552 | 0.2041 | $4D_{5/2} \rightarrow 4F_{5/2}$ | 0.549 | 0.0510 | 0.0584 |
| $4D_{3/2} \rightarrow 6P_{3/2}$ | -0.120 | 0.0033 | 0.0026 | $4D_{5/2} \rightarrow 5F_{5/2}$ | -0.209 | 0.0056 | 0.0064 |
| $4D_{3/2} \rightarrow 7P_{3/2}$ | -0.058 | 0.0006 | 0.0005 | $4D_{5/2} \rightarrow 6F_{5/2}$ | 0.092 | 0.0010 | 0.0011 |
| $4D_{3/2} \rightarrow 8P_{3/2}$ | 0.036 | 0.0002 | 0.0002 | $4D_{5/2} \rightarrow 4F_{7/2}$ | -2.461 | 1.0231 | -0.3653 |
| $4D_{3/2} \rightarrow 9P_{3/2}$ | 0.025 | 0.0001 | 0.0001 | $4D_{5/2} \rightarrow 5F_{7/2}$ | -0.960 | 0.1186 | -0.0424 |
| $4D_{3/2} \rightarrow 10P_{3/2}$ | -0.022 | 0.0001 | 0.0001 | $4D_{5/2} \rightarrow 6F_{7/2}$ | -0.466 | 0.0248 | -0.0089 |
| $4D_{3/2} \rightarrow 4F_{5/2}$ | -2.027 | 1.0320 | -0.2064 | | | | |
| $4D_{3/2} \rightarrow 5F_{5/2}$ | 0.779 | 0.1166 | -0.0233 | | | | |
| $4D_{3/2} \rightarrow 6F_{5/2}$ | -0.359 | 0.0219 | -0.0044 | | | | |
| $4D_{3/2} \rightarrow 7F_{5/2}$ | -0.170 | 0.0052 | -0.0010 | | | | |
| $4D_{3/2} \rightarrow 8F_{5/2}$ | 0.022 | 0.0001 | 0.0000 | | | | |
| $\alpha_{\text{Main}}^{\text{val}}$ | | 2.8584 | -1.4506 | $\alpha_{\text{Main}}^{\text{val}}$ | | 2.8698 | -1.9964 |
| $\alpha_{\text{Tail}}^{\text{val}}$ | | 0.1799 | -0.0419 | $\alpha_{\text{Tail}}^{\text{val}}$ | | 0.2519 | -0.0811 |
| α^{c} | | 3.0154 | | α^{c} | | 3.0154 | |
| α^{vc} | | -0.2726 | 0.1816 | α^{vc} | | -0.3002 | 0.3002 |
| Total | | 5.7811 | -1.3109 | Total | | 5.8369 | -1.7773 |
| $\delta(\%)$ | | 1.71 | 1.47 | $\delta(\%)$ | | 1.45 | 4.19 |

laser. Table II shows that the $4D_{3/2} \rightarrow 5P_{1/2,3/2}$ and $4D_{3/2} \rightarrow (4, 5)F_{5/2}$ transitions again contribute significantly to the main part of the valence polarizability of the $4D_{3/2}$ state for a pumping laser of 216.44 nm. Furthermore, in the case of dynamic dipole polarizability of the $4D_{5/2}$ state, it can be seen that the $4D_{5/2} \rightarrow 5P_{3/2}$ and $4D_{5/2} \rightarrow (4, 5)F_{7/2}$ transitions are dominant and contribute greatly to $\alpha_{\text{Main}}^{\text{val}}$. It gives E1 polarizability values as 7.0919(1180) and 7.2587(1443) a.u. for the $M_J = \pm 1/2$ components of ground and excited states, respectively, with uncertainty less than 2% (estimated as the difference in the results from the RMBPT3 method).

B. M1 polarizability

The interaction of magnetic moments μ_m within an ion with external magnetic field leads to the induction of magnetic dipoles. This phenomenon of magnetic polarization can be described quantitatively by magnetic dipole polarizability α^{M1} . Defining the M1 operator $\hat{O}^{\text{M1}} = (\mathbf{L} + 2\mathbf{S})\mu_B$ for Russell-Saunders coupling, with \mathbf{L} and \mathbf{S} being orbital and spin angular momentum operators, we can further calculate the magnetic dipole polarizability for any level $|J_v, M_J\rangle$ by

$$\alpha_v^{\text{M1}} = -\frac{2}{3(2J_v + 1)} \sum_k \frac{|\langle J_v || \hat{O}^{\text{M1}} || J_k \rangle|^2}{E_v - E_k}, \quad (12)$$

where J_k represents the intermediate states to which all the allowed transitions from J_v are possible.

Unlike E1 polarizabilities, the evaluation of the α^{M1} values is highly dominated by the contributions from the transitions involving the fine-structure partners. Thus, we estimate α^{M1} values of the $4D_{3/2}$ and $4D_{5/2}$ states by considering the M1 amplitude between these two states, and they are found to be $1.3940(92) \times 10^{-27}$ and $-9.2925(600) \times 10^{-28} \text{ J T}^{-2}$, respectively. In this case, we see uncertainties of 0.1% and 6% in comparison to the values obtained using the RMBPT3 method.

V. FREQUENCY SHIFTS

In order to calculate various systematic shifts in the proposed clock transition, we use E1 and M1 polarizabilities of the involved states, as discussed above. An analysis and discussion of the major systematic shifts in the proposed clock frequency measurement are given below (see Table III).

A. BBR shifts

Thermal fluctuations of the electromagnetic field experienced by an ion due to the temperature T of the surrounding environment are prevalent and need to be considered. At room temperature, the interactions of the system with both electric- and magnetic-field components of blackbody radiation lead to shifts in the energy states that are known as BBR Stark and BBR Zeeman shifts, respectively. They are one of the major irreducible contributions to the uncertainty of any atomic clock [47,48]. The generalized formula for the energy shift due to

TABLE III. Estimated systematic shifts in the $4D_{3/2}-4D_{5/2}$ clock transition of the Zr^{3+} ion.

| Source | $\Delta\nu$ (Hz) | $\frac{\Delta\nu}{\nu_0}$ |
|---|---------------------------|---------------------------|
| Electric quadrupole ($\frac{\partial \mathcal{E}_z}{\partial z} = 10^6$ V/m ²) | -0.03884 | -1.0353×10^{-15} |
| BBR Stark ($T = 300$ K) | -6.5524×10^{-4} | -1.7464×10^{-17} |
| BBR Zeeman ($T = 300$ K) | 1.3443×10^{-5} | 3.5829×10^{-19} |
| ac Stark (216.44 nm) | -1.6527×10^{-8} | -4.4048×10^{-22} |
| Quadratic Zeeman ($B = 10^{-8}$ T) | 1.7521×10^{-10} | 4.5978×10^{-24} |
| Second-order Doppler (thermal) | -4.6007×10^{-15} | -1.2262×10^{-28} |

blackbody radiation is given by [47]

$$\Delta E_v = -\frac{(\alpha_{fs} k_B T)^{(2L+1)}}{2J_v + 1} \sum_{k \neq v} |\langle \psi_v | \hat{O} | \psi_k \rangle|^2 F_L \left(\frac{\omega_{kv}}{k_B T} \right), \quad (13)$$

where \hat{O} are the multipolar electromagnetic transition operators (which can be either E1 or M1 operators), α_{fs} is the fine-structure constant, L is the orbital angular momentum, J_v is the total angular momentum of state v , and k_B is the Boltzmann constant. Here, $\omega_{kv} = \omega_v - \omega_k$ corresponds to the difference in angular frequencies of the two levels. In Eq. (13), replacing $\frac{\omega_{kv}}{k_B T}$ with y , the Farley-Wing function $F_L(y)$ can be written as [49]

$$F_L(y) = \frac{1}{\pi} \frac{L+1}{L(2L+1)!!(2L-1)!!} \times \int_0^\infty \left(\frac{1}{y+x} + \frac{1}{y-x} \right) \frac{x^{(2L+1)}}{e^x - 1} dx. \quad (14)$$

Further, the frequency shifts in state v due to the E1 and M1 channels can be given in terms of electric and magnetic dipole polarizabilities, respectively. At $T = 300$ K, the BBR Stark shift can be expressed in terms of the differential static scalar polarizability $\Delta\alpha_0^{E1} = \alpha_{v0}^{E1} - \alpha_{w0}^{E1}$ of the considered clock transition as [50]

$$\Delta\nu_{\text{BBR}}^{E1} = -\frac{1}{2} (831.9 \text{ V/m})^2 \Delta\alpha_0^{E1}. \quad (15)$$

In Eq. (15), the polarizability α in atomic units can be converted into SI units via $\alpha/h [\text{Hz}(\text{V/m})^{-2}] = 2.48832 \times 10^{-8} \alpha$ (a.u.). On the other hand, the BBR Zeeman Shift through allowed M1 transitions from the ground state is expressed as [51]

$$\Delta\nu_{\text{BBR}}^{M1} = -\frac{1}{2h} (2.77 \times 10^{-6} \text{ T})^2 \Delta\alpha^{M1} \quad (16)$$

for $T = 300$ K. Here, $\Delta\alpha^{M1}$ is the differential magnetic polarizability of the considered clock transition and can be calculated using Eq. (12) for our THz clock transition. Also, α^{M1} in terms of the Bohr magneton can be converted into SI units by using the relation $1\mu_B = 9.274 \times 10^{-24} \text{ JT}^{-1}$.

The individual contributions of the dominant transitions in the static dipole polarizabilities of the considered clock states are enlisted in Table I. α_{w0}^{E1} for $|4D_{3/2}, \pm 1/2\rangle$ and α_{v0}^{E1} for $|4D_{5/2}, \pm 1/2\rangle$ are estimated to be 6.1162 and 6.0351 a.u., respectively. Therefore, the differential static scalar electric dipole polarizability ($\Delta\alpha_0^{E1}$) of 0.0761 a.u. for these states gives a total BBR Stark shift $\Delta\nu_{\text{BBR}}^{E1}$ of -6.5524×10^{-4} Hz

at temperature $T = 300$ K. This leads to the fractional shift of -1.7464×10^{-17} in the clock transition. Further, the magnetic dipole polarizabilities α^{M1} for the $|4D_{3/2}, \pm 1/2\rangle$ and $|4D_{5/2}, \pm 1/2\rangle$ states are estimated to be 1.3940×10^{-27} and $-9.2925 \times 10^{-28} \text{ JT}^{-2}$, respectively, using Eq. (12). Substituting the values in Eq. (16), we get the net BBR Zeeman shift of 1.3443×10^{-5} Hz, which further gives the fractional frequency shift of 3.5829×10^{-19} at 300 K. Since this shift is directly proportional to $(\frac{T(\text{K})}{300\text{K}})^4$, the BBR shift can largely be suppressed by cooling the clock.

B. AC Stark shifts

The interaction of external electric fields with clock states leads to an ac Stark shift within them. This ac Stark shift greatly depends on the dynamic dipole polarizabilities of the considered states in the presence of these external electric fields. The dynamic dipole polarizabilities of these states can be calculated by using Eq. (8). Consequently, the corresponding ac Stark shift for a transition occurring between states w and v is given by [52]

$$\Delta\nu_{\text{Stark}} = -\frac{1}{2\pi} \left(\frac{\mathcal{E}}{2} \right)^2 \Delta\alpha^{E1}, \quad (17)$$

where $\Delta\alpha^{E1}$ is the differential dynamic polarizability given by $\Delta\alpha^{E1} = \alpha_v^{E1} - \alpha_w^{E1}$.

We evaluate the total dynamic dipole polarizabilities of the ground and excited states to be 7.0919 and 7.2587 a.u., respectively. Since the $4D_{3/2}-5S_{1/2}$ transition is a near-resonant transition, the detuning frequency and frequency fluctuations for a 261.38-nm pumping laser can cause an ac Stark shift in the $4D_{3/2}$ state. This can be avoided by introducing a pulse-light sequence [53]. Moreover, this shift can easily be controlled if the 261.38-nm laser is narrowed by the Pound-Drever-Hall technique and is well locked to the 261.38-nm transition [54,55]. Nonetheless, assuming an electric field \mathcal{E} of 10 V/m [56], we estimate the ac Stark shift in the clock frequency due to the 216.44-nm pumping laser to be -1.6342×10^{-8} Hz. This gives a fractional shift in the clock frequency of -4.3555×10^{-22} .

C. Zeeman shifts

In the presence of external magnetic field B , atomic energy levels and transition frequencies experience a Zeeman shift which, in fact, arises when the atomic magnetic dipole moment μ_m interacts with the external magnetic field [57]. A linear Zeeman shift can be avoided if the average is taken

over the transition frequencies with positive and negative M_J states, as described in Refs. [58,59]. Although a first-order Zeeman shift is avoidable, the quadratic Zeeman shift contributes greatly to the frequency uncertainty budget and hence must be considered. Further, the quadratic Zeeman shift can be expressed in terms of the differential magnetic dipole polarizability $\Delta\alpha^{M1}$ as [60]

$$\Delta\nu^{(Z2)} = -\frac{1}{2h}\Delta\alpha^{M1}\mathcal{B}^2, \quad (18)$$

with $\Delta\alpha^{M1} = \alpha_v^{M1} - \alpha_w^{M1}$. In Eq. (18), the magnetic polarizability for the corresponding states can be evaluated using Eq. (12).

The quadratic Zeeman shift is large enough to be considered for the analysis of the systematics of the clock system. Therefore, the only considerable Zeeman shift in our study is second order, which can further be determined by evaluating the magnetic dipole polarizabilities α^{M1} of the involved states using Eq. (12). These values are thus substituted for the determination of the second-order Zeeman shift using Eq. (18). The estimated values of α^{M1} for the considered states as stated in Sec. V A lead to $\Delta\nu^{(Z2)}$ and $\frac{\Delta\nu^{(Z2)}}{\nu_0}$ of 1.7521×10^{-10} Hz and 4.5978×10^{-24} , respectively, for $\mathcal{B} = 10^{-8}$ T [61].

D. Electric quadrupole shifts

The electric quadrupole (EQ) shift is caused by the interaction of the quadrupole moments of the clock levels and a residual electric field gradient at the trap center [62–70]. The electric quadrupole shift can be expressed in terms of the electric field gradient $\frac{\partial\mathcal{E}_z}{\partial z}$ as [65,71]

$$\Delta\nu_{\text{EQ}} = -\frac{1}{2h}\Delta\Theta\frac{\partial\mathcal{E}_z}{\partial z}, \quad (19)$$

where $\Delta\Theta$ is the differential electric quadrupole moment [72]. We consider the typical value of the electric field gradient $\frac{\partial\mathcal{E}_z}{\partial z}$, which is 10^6 V/m² for traps [73]. Here, the quadrupole moment $\Theta(J_v)$ of an atom in the electronic state $|J_v, M_J\rangle$ can be expressed in terms of the quadrupole matrix element of the electric quadrupole operator \hat{O}^{E2} using the expression [74]

$$\Theta(J_v) = (-1)^{J_v - M_J} \begin{pmatrix} J_v & 2 & J_v \\ -M_J & 0 & M_J \end{pmatrix} \langle J_v || \hat{O}^{E2} || J_v \rangle. \quad (20)$$

Corresponding to $|4D_{3/2}, \pm 1/2\rangle$ and $|4D_{5/2}, \pm 1/2\rangle$ states, the quadrupole moments are estimated to be 0.7278 and 0.8426 a.u., respectively, using Eq. (20), which can be converted into SI units by $1ea_0^2 = 4.4866 \times 10^{-40}$ C m². These values of the quadrupole moments would lead to a quadrupole frequency shift of -0.0388 Hz and a fractional frequency shift of -1.0353×10^{-15} . Even though this quadrupole shift is very high, it can be eliminated by averaging the clock transition frequency over the three mutually orthogonal magnetic-field orientations, independent of the orientation of the electric-field gradient [65,75].

E. Doppler shift

Doppler shift occurs when cold, but moving, ions interact with a field inside the microwave cavity that has a spatial

phase variation which does not form purely a standing wave [76]. The first-order Doppler shift can be eliminated by using two probe beams in opposite directions for the detection [77]; however, the second-order Doppler shift due to secular motion is quite considerable and can be expressed in terms of the mass m of the ion and speed of light c in vacuum as [78]

$$\Delta\nu_{\text{D2}} = -\left(\frac{3\hbar\Gamma}{4mc^2}\right)\nu_0. \quad (21)$$

With the advancement in experimentation, cooling lasers under optimized working conditions are adopted for cooling the ion trap. The temperature of the ion trap is reduced to a value closer to the Doppler-cooling limit T_D , further reducing the second-order Doppler shift due to the secular motion of the ion [79]. This Doppler-cooling limit is determined using the formula [80]

$$T_D = \frac{\hbar\Gamma}{2k_B}, \quad (22)$$

where Γ is the rate of spontaneous emission of the excited state (Γ^{-1} is the excited-state lifetime), which is actually related to the natural linewidth of the atomic transition. If we insert the value of the Doppler-cooling limit from Eq. (22) into it, Eq. (21) is rewritten as

$$\Delta\nu_{\text{D2}} = -\left(\frac{3k_B T_D}{2mc^2}\right)\nu_0. \quad (23)$$

Since Γ is the inverse of the lifetime of the upper state τ_v , viz., $4D_{5/2}$ in the case of the Zr³⁺ ion, $\Gamma = \frac{1}{\tau_v} = 2.1106 \times 10^{-2}$ Hz, which further gives a Doppler-cooling limit of 0.0807 pK. Therefore, with the insertion of the value of T_D in Eq. (23), the second-order Doppler shift and fractional frequency shift are found to be -4.6007×10^{-15} Hz and -1.2262×10^{-28} , respectively.

VI. COMPARISON WITH OTHER PROSPECTIVE THz CLOCKS

Previous studies based on THz clock transitions suggested average fractional shifts of the order of 10^{-12} and 10^{-14} using Mg atoms [13] and Sr₂ vibrational transitions [25], respectively. In contrast, the Zr³⁺ clock transition shows an average fractional shift of the order of 10^{-16} . The fractional second-order Zeeman shifts calculated for chip-scale carbonyl sulfide clocks by Kim *et al.* [15] and Wang *et al.* [24] were found to be of the order of 10^{-11} (for 100 G) and 10^{-10} (for 75 G), respectively. The value in the undertaken Zr³⁺ ion clock is found to be extremely insensitive to external magnetic conditions, which is, in fact, an important factor for quantum thermometry.

VII. CONCLUSION

We demonstrated that the $|4D_{3/2}, M_J = \pm 1/2\rangle \rightarrow |4D_{5/2}, M_J = \pm 1/2\rangle$ transition in ⁹⁰Zr³⁺ can be used for a THz atomic clock. In this regard, the clock transition principle was discussed, and major systematics of this transition such as BBR, ac Stark, electric quadrupole, second-order Doppler, and second-order Zeeman shifts were estimated and compared

with other prospective THz clock candidates. We observed that the maximum contribution to the systematics of this transition is given by the electric quadrupole effect, which, in fact, can be eliminated by averaging the clock transition frequency over three mutually perpendicular directions of the electric field for a given magnetic field. Other shifts determined for this transition were found to be suppressed. After a comparative analysis with previously proposed THz clocks, fractional shifts in the Zr^{3+} ion were found to be much better. In a realistic experimental setup, they can be controlled further. Upon successful development of the proposed THz clock, it would be highly useful in quantum thermometry.

ACKNOWLEDGMENTS

Jyoti and B.A. thank Priti at the National Institute for Fusion Science, Gifu, Japan, for fruitful discussions and critical feedback. Research at the Perimeter Institute is supported in part by the government of Canada through the Department of Innovation, Science and Economic Development and by the Province of Ontario through the Ministry of Colleges and Universities. We acknowledge the ParamVikram 1000 HPC facility at the Physical Research Laboratory, Ahmedabad, India, for carrying out relativistic coupled-cluster calculations. Y.-m.Y. acknowledges the support from the National Key Research and Development Program of China (Grant No. 2021YFA1402104).

-
- [1] T. Rosenband, D. B. Hume, P. O. Schmidt, C. W. Chou, A. Brusch, L. Lorini, W. H. Oskay, R. E. Drullinger, T. M. Fortier, J. E. Stalnaker, S. A. Diddams, W. C. Swann, N. R. Newbury, W. M. Itano, D. J. Wineland, and J. C. Bergquist, Frequency ratio of Al^+ and Hg^+ single-ion optical clocks; metrology at the 17th decimal place, *Science* **319**, 1808 (2008).
- [2] T. E. Mehlstäubler, G. Grosche, C. Lisdat, P. O. Schmidt, and H. Denker, Atomic clocks for geodesy, *Rep. Prog. Phys.* **81**, 064401 (2018).
- [3] W. F. McGrew, X. Zhang, R. J. Fasano, S. A. Schäffer, K. Beloy, D. Nicolodi, R. C. Brown, N. Hinkley, G. Milani, M. Schioppo *et al.*, Atomic clock performance enabling geodesy below the centimetre level, *Nature (London)* **564**, 87 (2018).
- [4] S. Kolkowitz, I. Pikovski, N. Langellier, M. D. Lukin, R. L. Walsworth, and J. Ye, Gravitational wave detection with optical lattice atomic clocks, *Phys. Rev. D* **94**, 124043 (2016).
- [5] A. Loeb and D. Maoz, Using atomic clocks to detect gravitational waves, *arXiv:1501.00996*.
- [6] P. W. Graham, J. M. Hogan, M. A. Kasevich, and S. Rajendran, New Method for Gravitational Wave Detection with Atomic Sensors, *Phys. Rev. Lett.* **110**, 171102 (2013).
- [7] A. Derevianko and M. Pospelov, Hunting for topological dark matter with atomic clocks, *Nat. Phys.* **10**, 933 (2014).
- [8] V. A. Dzuba, V. V. Flambaum, and S. Schiller, Testing physics beyond the standard model through additional clock transitions in neutral ytterbium, *Phys. Rev. A* **98**, 022501 (2018).
- [9] N. Huntemann, M. Okhapkin, B. Lipphardt, S. Weyers, C. Tamm, and E. Peik, High-Accuracy Optical Clock based on the Octupole Transition in $^{171}\text{Yb}^+$, *Phys. Rev. Lett.* **108**, 090801 (2012).
- [10] C. W. Chou, D. B. Hume, J. C. J. Koelemeij, D. J. Wineland, and T. Rosenband, Frequency Comparison of Two High-Accuracy Al^+ Optical Clocks, *Phys. Rev. Lett.* **104**, 070802 (2010).
- [11] M. Tonouchi, Cutting-edge terahertz technology, *Nat. Photonics* **1**, 97 (2007).
- [12] C. Kulesa, Terahertz spectroscopy for astronomy: From comets to cosmology, *IEEE Trans. Terahertz Sci. Technol.* **1**, 232 (2011).
- [13] F. Strumia, A proposal for a new absolute frequency standard, using a Mg or Ca atomic beam, *Metrologia* **8**, 85 (1972).
- [14] E. B. Norrgard, S. P. Eckel, C. L. Holloway, and E. L. Shirley, Quantum blackbody thermometry, *New J. Phys.* **23**, 033037 (2021).
- [15] M. Kim, C. Wang, Z. Hu, and R. Han, Chip-scale terahertz carbonyl sulfide clock: An overview and recent studies on long-term frequency stability of OCS transitions, *IEEE Trans. Terahertz Sci. Technol.* **9**, 349 (2019).
- [16] T. Yasui, S. Yokoyama, H. Inaba, K. Minoshima, T. Nagatsuma, and T. Araki, Terahertz frequency metrology based on frequency comb, *IEEE J. Sel. Top. Quantum Electron.* **17**, 191 (2010).
- [17] L. Consolino, S. Bartalini, and P. De Natale, Terahertz frequency metrology for spectroscopic applications: A review, *J. Infrared, Millimeter, Terahertz Waves* **38**, 1289 (2017).
- [18] M. Bellini, P. De Natale, G. Di Lonardo, L. Fusina, M. Inguscio, and M. Prevedelli, Tunable far infrared spectroscopy of $^{16}\text{O}_3$ ozone, *J. Mol. Spectrosc.* **152**, 256 (1992).
- [19] T. Yamamoto, H. Takara, and S. Kawanishi, Generation and transmission of tunable terahertz optical clock, in *International Topical Meeting on Microwave Photonics, Awaji, Japan* (IEEE, 2002).
- [20] X. Zhou, X. Xu, X. Chen, and J. Chen, Magic wavelengths for terahertz clock transitions, *Phys. Rev. A* **81**, 012115 (2010).
- [21] G.-H. Yu, Y.-G. Geng, L. Li, C. Zhou, C.-B. Duan, R.-P. Chai, and Y.-M. Yang, The ac Stark shifts of the terahertz clock transitions of barium, *Chin. Phys. B* **24**, 103201 (2015).
- [22] C. Wang, X. Yi, J. Mawdsley, M. Kim, Z. Wang, and R. Han, An on-chip fully electronic molecular clock based on sub-terahertz rotational spectroscopy, *Nat. Electron.* **1**, 421 (2018).
- [23] T. E. Drake, T. C. Briles, J. R. Stone, D. T. Spencer, D. R. Carlson, D. D. Hickstein, Q. Li, D. Westly, K. Srinivasan, S. A. Diddams, and S. B. Papp, Terahertz-Rate Kerr-Microresonator Optical Clockwork, *Phys. Rev. X* **9**, 031023 (2019).
- [24] C. Wang, X. Yi, M. Kim, Q. B. Yang, and R. Han, A terahertz molecular clock on CMOS using high-harmonic-order interrogation of rotational transition for medium-/long-term stability enhancement, *IEEE J. Solid-State Circuits* **56**, 566 (2020).
- [25] K. H. Leung, B. Iritani, E. Tiberi, I. Majewska, M. Borkowski, R. Moszynski, and T. Zelevinsky, Terahertz Vibrational Molecular Clock with Systematic Uncertainty at the 10^{-14} Level, *Phys. Rev. X* **13**, 011047 (2023).
- [26] Jyoti, M. Kaur, B. Arora, and B. K. Sahoo, Spectroscopic data of Rb-isoelectronic Zr and Nb ions for astrophysical applications, *Mon. Not. R. Astron. Soc.* **507**, 4030 (2021).

- [27] A. Das, A. Bhowmik, N. N. Dutta, and S. Majumder, Electron-correlation study of Y III-Tc VII ions using a relativistic coupled-cluster theory, *J. Phys. B* **51**, 025001 (2017).
- [28] M. Nomura, K. Kogure, and M. Okamoto, Isotopic abundance ratios and atomic weight of zirconium, *Int. J. Mass Spectrom. Ion Phys.* **50**, 219 (1983).
- [29] J. D. Silver, A. J. Varney, H. S. Margolis, P. E. G. Baird, I. P. Grant, P. D. Groves, W. A. Hallett, A. T. Handford, P. J. Hirst, A. R. Holmes *et al.*, The oxford electron-beam ion trap: A device for spectroscopy of highly charged ions, *Rev. Sci. Instrum.* **65**, 1072 (1994).
- [30] N. Nakamura, H. Kikuchi, H. A. Sakaue, and T. Watanabe, Compact electron beam ion trap for spectroscopy of moderate charge state ions, *Rev. Sci. Instrum.* **79**, 063104 (2008).
- [31] A. N. Agnihotri, A. H. Kelkar, S. Kasthurirangan, K. V. Thulasiram, C. A. Desai, W. A. Fernandez, and L. C. Tribedi, An ECR ion source-based low-energy ion accelerator: Development and performance, *Phys. Scr.* **T144**, 014038, (2011).
- [32] S. Hannig, L. Pelzer, N. Scharnhorst, J. Kramer, M. Stepanova, Z. T. Xu, N. Spethmann, I. D. Leroux, T. E. Mehlstäubler, and P. O. Schmidt, Towards a transportable aluminium ion quantum logic optical clock, *Rev. Sci. Instrum.* **90**, 053204 (2019).
- [33] B. Merkel, K. Thirumalai, J. E. Tarlton, V. M. Schäfer, C. J. Ballance, T. P. Harty, and D. M. Lucas, Magnetic field stabilization system for atomic physics experiments, *Rev. Sci. Instrum.* **90**, 044702 (2019).
- [34] S. A. Blundell, W. R. Johnson, and J. Sapirstein, Relativistic all-order calculations of energies and matrix elements in cesium, *Phys. Rev. A* **43**, 3407 (1991).
- [35] E. Eliav (Ilyabaev), U. Kaldor, and Y. Ishikawa, Relativistic coupled cluster method based on Dirac—Coulomb—Breit wavefunctions. ground state energies of atoms with two to five electrons, *Chem. Phys. Lett.* **222**, 82 (1994).
- [36] E. Lindroth and A. Ynnerman, *Ab initio* calculations of g_j factors for Li, Be⁺, and Ba⁺, *Phys. Rev. A* **47**, 961 (1993).
- [37] B. K. Sahoo, S. Majumder, R. K. Chaudhuri, B. P. Das, and D. Mukherjee, *Ab initio* determination of the lifetime of the 6²P_{3/2} state for ²⁰⁷Pb⁺ by relativistic many-body theory, *J. Phys. B* **37**, 3409 (2004).
- [38] D. K. Nandy and B. K. Sahoo, Quadrupole shifts for the ¹⁷¹Yb⁺ ion clocks: Experiments versus theories, *Phys. Rev. A* **90**, 050503(R) (2014).
- [39] J. Čížek, On the use of the cluster expansion and the technique of diagrams in calculations of correlation effects in atoms and molecules, *Adv. Chem. Phys.* **14**, 35 (1969).
- [40] U. I. Safronova, W. R. Johnson, M. S. Safronova, and A. Derevianko, Relativistic many-body calculations of transition probabilities for the 2l₁2l₂[LSJ]-2l₃2l₄[L'S'J'] lines in Be-like ions, *Phys. Scr.* **59**, 286 (1999).
- [41] C.-B. Li, Y.-M. Yu, and B. K. Sahoo, Relativistic coupled-cluster-theory analysis of energies, hyperfine-structure constants, and dipole polarizabilities of Cd⁺, *Phys. Rev. A* **97**, 022512 (2018).
- [42] B. K. Sahoo, Coupled-cluster theory of parity nonconservation in atoms, Ph.D. thesis, Mangalore University, Karnataka, India, 2005.
- [43] E. Iskrenova-Tchoukova, M. S. Safronova, and U. I. Safronova, High-precision study of Cs polarizabilities, *J. Comput. Methods Sci. Eng.* **7**, 521 (2007).
- [44] A. Kramida, Y. Ralchenko, J. Reader, and NIST ASD Team, NIST Atomic Spectra Database, version 5.8, <https://physics.nist.gov/asd>.
- [45] N. L. Manakov, V. D. Ovsiannikov, and L. P. Rapoport, Atoms in a laser field, *Phys. Rep.* **141**, 320 (1986).
- [46] J. Kaur, D. K. Nandy, B. Arora, and B. K. Sahoo, Properties of alkali-metal atoms and alkaline-earth-metal ions for an accurate estimate of their long-range interactions, *Phys. Rev. A* **91**, 012705 (2015).
- [47] J. W. Farley and W. H. Wing, Accurate calculation of dynamic Stark shifts and depopulation rates of Rydberg energy levels induced by blackbody radiation. Hydrogen, helium, and alkali-metal atoms, *Phys. Rev. A* **23**, 2397 (1981).
- [48] Y.-M. Yu and B. K. Sahoo, Selected highly charged ions as prospective candidates for optical clocks with quality factors larger than 10¹⁵, *Phys. Rev. A* **97**, 041403(R) (2018).
- [49] S. G. Porsev and A. Derevianko, Multipolar theory of blackbody radiation shift of atomic energy levels and its implications for optical lattice clocks, *Phys. Rev. A* **74**, 020502(R) (2006).
- [50] B. Arora, M. S. Safronova, and C. W. Clark, Blackbody-radiation shift in a ⁴³Ca⁺ ion optical frequency standard, *Phys. Rev. A* **76**, 064501 (2007).
- [51] B. Arora, D. K. Nandy, and B. K. Sahoo, Multipolar blackbody radiation shifts for single-ion clocks, *Phys. Rev. A* **85**, 012506 (2012).
- [52] K. Beloy, Theory of the ac Stark effect on the atomic hyperfine structure and applications to microwave atomic clocks, Ph.D. thesis, University of Nevada, Reno, 2009.
- [53] Y. Huang, Q. Liu, J. Cao, B. Ou, P. Liu, H. Guan, X. Huang, and K. Gao, Evaluation of the systematic shifts of a single-⁴⁰Ca⁺ ion frequency standard, *Phys. Rev. A* **84**, 053841 (2011).
- [54] R. W. P. Drever, J. L. Hall, F. V. Kowalski, J. Hough, G. M. Ford, A. J. Munley, and H. Ward, Laser phase and frequency stabilization using an optical resonator, *Appl. Phys. B* **31**, 97 (1983).
- [55] E. D. Black, An introduction to Pound–Drever–Hall laser frequency stabilization, *Am. J. Phys.* **69**, 79 (2001).
- [56] Y.-M. Yu and B. K. Sahoo, Scrutinizing Al-like ⁵¹V¹⁰⁺, ⁵³Cr¹¹⁺, ⁵⁵Mn¹²⁺, ⁵⁷Fe¹³⁺, ⁵⁹Co¹⁴⁺, ⁶¹Ni¹⁵⁺, and ⁶³Cu¹⁶⁺ ions for atomic clocks with uncertainties below the 10⁻¹⁹ level, *Phys. Rev. A* **94**, 062502 (2016).
- [57] C. J. Campbell, A. G. Radnaev, A. Kuzmich, V. A. Dzuba, V. V. Flambaum, and A. Derevianko, Single-Ion Nuclear Clock for Metrology at the 19th Decimal Place, *Phys. Rev. Lett.* **108**, 120802 (2012).
- [58] V. A. Dzuba, S. O. Allehabi, V. V. Flambaum, J. Li, and S. Schiller, Time keeping and searching for new physics using metastable states of Cu, Ag, and Au, *Phys. Rev. A* **103**, 022822 (2021).
- [59] M. Takamoto, F.-L. Hong, R. Higashi, Y. Fujii, M. Imae, and H. Katori, Improved frequency measurement of a one-dimensional optical lattice clock with a spin-polarized fermionic ⁸⁷Sr isotope, *J. Phys. Soc. Jpn.* **75**, 104302 (2006).
- [60] S. G. Porsev and M. S. Safronova, Calculation of higher-order corrections to the light shift of the 5s²1S₀-5s5p³P₀^o clock transition in Cd, *Phys. Rev. A* **102**, 012811 (2020).
- [61] A. Derevianko, V. A. Dzuba, and V. V. Flambaum, Highly Charged Ions as a Basis of Optical Atomic Clockwork of Exceptional Accuracy, *Phys. Rev. Lett.* **109**, 180801 (2012).

- [62] T. Udem, S. A. Diddams, K. R. Vogel, C. W. Oates, E. A. Curtis, W. D. Lee, W. M. Itano, R. E. Drullinger, J. C. Bergquist, and L. Hollberg, Absolute Frequency Measurements of the Hg^+ and Ca Optical Clock Transitions with a Femtosecond Laser, *Phys. Rev. Lett.* **86**, 4996 (2001).
- [63] J. Stenger, C. Tamm, N. Haverkamp, S. Weyers, and H. R. Telle, Absolute frequency measurement of the 435.5-nm $^{171}\text{Yb}^+$ -clock transition with a Kerr-lens mode-locked femtosecond laser, *Opt. Lett.* **26**, 1589 (2001).
- [64] H. S. Margolis, G. P. Barwood, G. Huang, H. A. Klein, S. N. Lea, K. Szymaniec, and P. Gill, Hertz-level measurement of the optical clock frequency in a single $^{88}\text{Sr}^+$ ion, *Science* **306**, 1355 (2004).
- [65] W. M. Itano, External-field shifts of the $^{199}\text{Hg}^+$ optical frequency standard, *J. Res. Natl. Inst. Stand. Technol.* **105**, 829 (2000).
- [66] A. A. Madej, J. E. Bernard, P. Dubé, L. Marmet, and R. S. Windeler, Absolute frequency of the $^{88}\text{Sr}^+5s^2S_{1/2}-4d^2D_{5/2}$ reference transition at 445 THz and evaluation of systematic shifts, *Phys. Rev. A* **70**, 012507 (2004).
- [67] G. P. Barwood, H. S. Margolis, G. Huang, P. Gill, and H. A. Klein, Measurement of the Electric Quadrupole Moment of the $4d^2D_{5/2}$ Level in $^{88}\text{Sr}^+$, *Phys. Rev. Lett.* **93**, 133001 (2004).
- [68] U. Tanaka, S. Bize, C. E. Tanner, R. E. Drullinger, S. A. Diddams, L. Hollberg, W. M. Itano, D. J. Wineland, and J. C. Bergquist, The $^{199}\text{Hg}^+$ single ion optical clock: Recent progress, *J. Phys. B* **36**, 545 (2003).
- [69] T. Schneider, C. Tamm, and E. Peik, Comparison of two single-ion optical frequency standards at the Hertz level, *Proceedings of the 2003 IEEE International Frequency Control Symposium and PDA Exhibition Jointly with the 17th European Frequency and Time Forum, Tampa, FL* (IEEE, 2003), pp. 72–74.
- [70] W. H. Oskay, W. M. Itano, and J. C. Bergquist, Measurement of the $^{199}\text{Hg}^+5d^96s^{22}D_{5/2}$ Electric Quadrupole Moment and a Constraint on the Quadrupole Shift, *Phys. Rev. Lett.* **94**, 163001 (2005).
- [71] S. G. Porsev, U. I. Safronova, M. S. Safronova, P. O. Schmidt, A. I. Bondarev, M. G. Kozlov, I. I. Tupitsyn, and C. Cheung, Optical clocks based on the Cf^{15+} and Cf^{17+} ions, *Phys. Rev. A* **102**, 012802 (2020).
- [72] N. Ramsey, *Molecular Beams*, International Series of Monographs on Physics (Oxford University Press, Oxford, 1985).
- [73] A. Kozlov, V. A. Dzuba, and V. V. Flambaum, Prospects of building optical atomic clocks using Er I or Er III, *Phys. Rev. A* **88**, 032509 (2013).
- [74] C. Sur, K. V. P. Latha, B. K. Sahoo, R. K. Chaudhuri, B. P. Das, and D. Mukherjee, Electric Quadrupole Moments of the d States of Alkaline-Earth-Metal Ions, *Phys. Rev. Lett.* **96**, 193001 (2006).
- [75] P. Dubé, A. A. Madej, J. E. Bernard, L. Marmet, J.-S. Boulanger, and S. Cundy, Electric Quadrupole Shift Cancellation in Single-Ion Optical Frequency Standards, *Phys. Rev. Lett.* **95**, 033001 (2005).
- [76] J. Guéna, R. Li, K. Gibble, S. Bize, and A. Clairon, Evaluation of Doppler Shifts to Improve the Accuracy of Primary Atomic Fountain Clocks, *Phys. Rev. Lett.* **106**, 130801 (2011).
- [77] D. J. Wineland, Nobel lecture: Superposition, entanglement, and raising Schrödinger's cat, *Rev. Mod. Phys.* **85**, 1103 (2013).
- [78] J. Zhang, K. Deng, J. Luo, and Z.-H. Lu, Direct laser cooling of ion optical clocks, *Chin. Phys. Lett.* **34**, 050601 (2017).
- [79] Y. Huang, B. Zhang, M. Zeng, Y. Hao, Z. Ma, H. Zhang, H. Guan, Z. Chen, M. Wang, and K. Gao, Liquid-Nitrogen-Cooled Ca^+ Optical Clock with Systematic Uncertainty of 3×10^{-18} , *Phys. Rev. Appl.* **17**, 034041 (2022).
- [80] W. D. Phillips, Nobel lecture: Laser cooling and trapping of neutral atoms, *Rev. Mod. Phys.* **70**, 721 (1998).